

Revealing Non-covalent Interactions in Molecular Crystals through Their Experimental Electron Densities

Gabriele Saleh,^[a, c] Carlo Gatti,^{*, [b, c]} Leonardo Lo Presti,^{*, [a, b, c]} and Julia Contreras-García^[d]

Abstract: Non-covalent interactions (NCI) define the rules underlying crystallisation, self-assembly and drug–receptor docking processes. A novel NCI descriptor, based on the reduced electron density gradient (RDG), that enables easy visualisation of the zones of the electron density (ED) involved in either the supposedly attractive (dispersive, hydrogen bonding) or allegedly repulsive (steric) intermolecular interactions, was recently developed by Johnson et al. Here, it is applied for the first time to EDs derived from single-crystal X-ray diffraction data. A computer code handling both experimental and ab initio EDs in the RDG-NCI perspective was purposely written. Three cases spanning a wide range of

NCI classes were analysed: 1) benzene, as the prototype of stacking and weak CH \cdots π interactions; 2) austdiol, a heavily functionalised fungal metabolite with a complex hydrogen-bonding network; 3) two polymorphs of the heteroatom-rich anti-ulcer drug famotidine, with van der Waals and hydrogen-bond contacts between N- and S-containing groups. Even when applied to experimental EDs, the RDG index is a valuable NCI descriptor that can highlight their different nature and strength and

provide results of comparable quality to ab initio approaches. Combining the RDG-NCI study with Bader's ED approach was a key step forward, as the RDG index can depict inherently delocalised interactions in terms of extended and flat RDG isosurfaces, in contrast to the bond path analysis, which is often bounded to a too localised and possibly discontinuous (yes/no) description. Conversely, the topological tool can provide quantitative insight into the simple, qualitative NCI picture offered by the RDG index. Hopefully, this study may pave the way to a deeper analysis of weak interactions in proteins using structural and ED information from experiment.

Keywords: noncovalent interactions · quantum chemistry · reduced density gradient · solid-state structures · X-ray diffraction

Introduction

Non-covalent interactions (NCI) are of paramount importance in chemistry and especially in bio-disciplines,^[1,2] since they set up the force-field scenario through which chemical species interact with each other without a significant electron sharing between them. They represent, in fact, the machinery through which molecules *recognise* themselves and establish how molecules will approach and eventually pack together. The NCIs encompass several bonding types, such as hydrogen bonds (HBs), halogen bonds, CH \cdots π and $\pi\cdots\pi$ interactions and several binding (or anti-binding) forces, like those due to dispersion, electrostatics or to Pauli's principle. The latter is related to the customary classification of closed-shell interactions among neutral species as short-range (steric) repulsions,^[1] though these species may also be globally stabilised by the competing and prevailing effect of other binding mechanisms.


During the last decade, NCIs have raised a great deal of interest in the context of gaining insight into self-assembly^[3] and crystallisation^[4] processes, whose underlying general rules are still far from being fully rationalised and understood.^[5] Though their knowledge would in principle allow to build from scratch (even complex) materials exhibiting the desired properties,^[6–8] it can not be ignored that a given ob-

[a] M. Sc. G. Saleh, Dr. L. Lo Presti
Università degli Studi di Milano, Dipartimento di Chimica
Via Golgi 19, 20133 Milano (Italy)
Fax: (+39)02-50314300
E-mail: leonardo.lopresti@unimi.it

[b] Dr. C. Gatti, Dr. L. Lo Presti
Istituto di Scienze e Tecnologie Molecolari del CNR (CNR-ISTM)
Via Golgi 19, 20133 Milano (Italy)
Fax: (+39)02-50314300
E-mail: c.gatti@istm.cnr.it

[c] M. Sc. G. Saleh, Dr. C. Gatti, Dr. L. Lo Presti
Center for Materials Crystallography, Aarhus University
Langelandsgade 140, 8000 Aarhus (Denmark)

[d] Dr. J. Contreras-García
Laboratoire de Chimie Théorique, Université Pierre et Marie Curie
4 Pl Jussieu, 75005 Paris (France)

 Supporting information for this article (S1: details of multipole refinements; S2: details of periodic calculations; S3: details of the new code for evaluating RDG isosurfaces from experimental X-ray densities; S4: grid step, cut-offs and other choices regarding RDG isosurfaces; S5: comparison of RDG isosurfaces and BCP data as obtained from experiment and theory) is available on the WWW under <http://dx.doi.org/10.1002/chem.201201290>.

served structure is generally the outcome of a “draw” among a plethora of energetically similar, but structurally dissimilar options, with the end result being very often driven more by kinetic than by thermodynamic considerations alone.^[9] Understanding intermolecular non-covalent interactions and their mutual interplay in supramolecular assemblies is nonetheless a fundamental step in making progress in structural prediction and evolution.

Nowadays, several theoretical and experimental methods exist for investigating intermolecular NCI. For example, it is possible to analyze the contact geometries of atoms belonging to different molecules in the bulk, as they are retrieved by single crystal X-ray diffraction experiments,^[10] looking for frequent packing modes and possible trends along chemically related substances^[5] or by analysing such atom contacts in a more sophisticated and enlightening way by using the so-called Hirshfeld surfaces of the interacting molecules.^[11] Interaction or packing energies, that is, the changes in the electronic energy of the molecule due to its gas-phase or crystalline surroundings, can be computed either quantum mechanically^[12] or by suitable empirical atom–atom potentials,^[13] and with a plethora of different recipes.^[5,12] On top of this, the electron density (ED) observable $\rho(\mathbf{r})$, which may be obtained from ab initio methods as well as from single-crystal X-ray diffraction, contains a huge amount of information on how molecules in close contact influence each other and may thus be employed also for revealing intermolecular NCI. Being based on a quantum observable and (easily) measurable quantity, the ED-based descriptors retain the great advantage of enabling comparison of theoretical predictions with experimental results on the same grounds. During the last 20 years, several studies have been devoted to such comparisons,^[14–16] as well as to the aim of correlating experimental and theoretical ED topology with hydrogen bond energies,^[17–19] or with interaction^[20–22] or packing energies^[22–24] due to other weak bonds. In recent decades, topological analysis of $\rho(\mathbf{r})$ has indeed become an established, standard tool to explore chemical bonding, within the framework of the quantum theory of atoms in molecules (QTAIM).^[25]

Despite its well-recognised ability to extract deep chemical insights from the ED,^[26,27] the QTAIM topological picture unavoidably provides an atom–atom pair, often “localised”^[28] and possibly discontinuous portrait of the chemical bond,^[29–31] whereas many significant non-covalent interactions have an inherently “delocalised” character^[32], and all chemical interactions are by nature characterised by continuous energy-contribution changes^[33] upon lengthening or shortening.^[30] Therefore, use of new NCI descriptors that can extend and reconcile the pure ED topological picture with that suggested by common chemical sense and corroborated by other one- and two-electron-based descriptors like the Source Function^[34,35] and the delocalisation indices, respectively,^[36] appears to be a real necessity.

In this context, we apply here, for the first time to experimentally derived multipole EDs in molecular solids, the ED-based NCI descriptor recently introduced by Johnson

et al.^[37] and Contreras-García et al.^[38,39] At variance with the QTAIM approach (see below), the latter is based on surfaces of constant (low) values of the reduced density gradient $s(\mathbf{r})$ that can be more or less extended in space. Indeed, they provide an easy-to-grasp pictorial representation of NCI and, when combined with the sign of the second principal local curvature of the ED, they allow both the supposedly attractive or repulsive nature of the interactions to be identified and their relative strength to be qualitatively ranked.

In the present work, we check the suitability of this new NCI descriptor when applied to multipole-derived charge densities, which are known to be possibly biased because of the arbitrariness inherent to the multipole refinement step.^[14,15] However, though clearly suffering also from the constraint of the limited data set and the often insufficient data quality, they have also the advantage of possibly avoiding some of the limitations inherent to those obtained from DFT, which is known to poorly describe NCI interactions in most cases. We therefore compared the results obtained from experimental EDs with those derived from the periodic wavefunction EDs. Then, we contrast the results of our NCI descriptor investigations with those obtained from classical QTAIM topological indicators, not only to highlight the analogies and differences between the two approaches, but especially to show how these descriptors may fruitfully complement each other, as they can, when combined, provide further insights into the NCI nature that would otherwise remain unveiled if used separately.

To perform such analysis, three different chemical systems, spanning a wide range of interaction classes, were chosen: 1) benzene,^[40] as a prototypical example of crystal packing dominated by interactions involving aromatic π electrons; 2) austdiol,^[41] a heavily functionalised fungal metabolite exhibiting quite a complex hydrogen bonding network, consisting of OH...O and CH...O interactions of different strength; 3) two polymorphs of the heteroatom-rich anti-ulcer drug famotidine,^[42] which both display several van der Waals and hydrogen-bond contacts between N- and S-containing groups.

The NCI descriptor: The method for evaluating intermolecular NCI proposed by Johnson et al.^[37] is based on the reduced density gradient (RDG) $s(\mathbf{r})$, a dimensionless quantity within the generalised gradient approximation of exchange-correlation term in DFT Hamiltonians [Eq. (1)].^[43,44]

$$s(\mathbf{r}) = \frac{|\nabla\rho(\mathbf{r})|}{2(3\pi^2)^{1/3}\rho(\mathbf{r})^{4/3}} \quad (1)$$

The RDG describes the local deviation of the charge density $\rho(\mathbf{r})$ from a homogeneous electron gas^[45] that has by definition null $s(\mathbf{r})$ everywhere. RDG assumes large values in regions far from the various nuclei of a system, where the total ED decays to zero exponentially and the $\rho(\mathbf{r})^{4/3}$ term approaches zero faster than $|\nabla\rho(\mathbf{r})|$. The lower bound of RDG is zero, reached whenever the ED gradient vanishes (e.g., at BCPs). Some years ago, the RDG was investigated

to improve the existing exchange-correlation functionals.^[44] Interestingly, it was found that the exchange energy weighted RDG (as defined in ref. [44]) diminishes on passing from isolated atoms to molecules and from molecules to crystals, which suggests that low RDG values could be associated with chemical interactions. Accordingly, Johnson et al.^[37] noticed that low-value RDG isosurfaces provide an easy-to-grasp representation of those zones of the ED distribution that are dominated by specific NCI^[46]. Moreover, by using the sign of the second largest eigenvalue λ_2 ($\lambda_1 \leq \lambda_2 \leq \lambda_3$) of the ED Hessian matrix at each isosurface point, they could distinguish between supposedly attractive ($\lambda_2 < 0$) and allegedly repulsive ($\lambda_2 > 0$) interactions. When the quantity $\rho(\mathbf{r}) \cdot \text{sign}(\lambda_2)$ is mapped onto the RDG isosurface, both the nature and strength of the interactions may be thus highlighted.^[37] Clearly, this NCI descriptor has points in common with the QTAIM ED topology, since a low-RDG isosurface will unavoidably appear in the neighbourhood of any CP, where the ED gradient vanishes by definition. Moreover, at the ED critical points, the Hessian eigenvalues correspond to the ED principal curvatures at these points, with λ_2 being negative and associated to an eigenvector perpendicular to the bond path at a BCP, and λ_2 being positive and associated to an eigenvector directed in the ring plane at a ring critical point.

To apply the RDG-based NCI descriptor to experimental EDs and to compare its performance against that using ab initio EDs, we wrote a Fortran90 code that reads ED grid and cube files provided by XD2006, Gaussian 09 and TOPOND program suites. A very concise description of the code is reported in Supporting Information S3, while its full details will be published elsewhere.^[47]

Results and Discussion

Applying the NCI descriptor to experimental electron densities: Operationally, we separately applied the NCI descriptor to a series of molecular pairs extracted from the crystal. This strategy implies that the contribution due to the multipoles centred on atoms belonging to the rest of the unit cell is ignored in reconstructing the multipole ED within each pair. In the Hansen–Coppens formalism^[48] implemented in the XD program package,^[49] the ED at each point \mathbf{r} can therefore be partitioned as follows [Eq. (2)]

$$\rho(\mathbf{r}) = \rho_A(\mathbf{r}) + \Delta\rho(\mathbf{r}) \quad (2)$$

where $\rho_A(\mathbf{r})$ is the contribution of a certain (group of) atom(s) or molecule(s) A and $\Delta\rho$ is that arising from the multipoles centred on the remaining atoms in the unit cell. In general, as the radial part of the multipole functions decays exponentially with $|\mathbf{r}|$,^[48] the *direct* contribution of an atom M , located at \mathbf{r}_M , to the ED at \mathbf{r} is negligible whenever the $|\mathbf{r} - \mathbf{r}_M|$ distance is significantly greater than the covalent radius of M . Accordingly, the main features of ED in the space between a pair of nearest neighbour molecules

depend almost exclusively on their (composing) pseudoatoms. We found that this condition was always satisfied in the present work, the only exception being that of a single benzene molecular pair (see below). Therefore, NCI analysis can in general be safely performed on a molecular pair extracted from the crystal, the effect of the crystalline matrix being properly and *indirectly* included in the multipole expansion of the molecular pair pseudoatoms.

Johnson et al. and Contreras-García et al.^[37,38] examined plots of s versus ρ for a number of simple isolated molecules and their homomolecular dimers in vacuo. These plots provide clear fingerprints of molecular and intermolecular interactions (e.g., see Figure 1 in ref. [37]). Figure 1a shows an

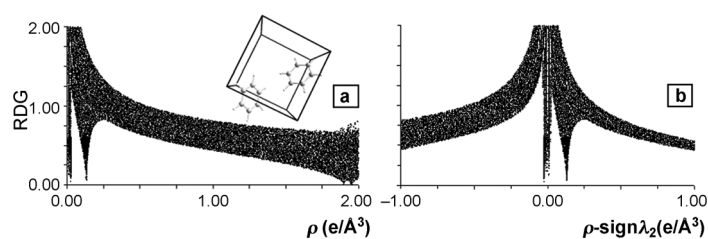


Figure 1. a) RDG versus ρ plots for two molecules of benzene at the crystal geometry. In the inset the representation of the region considered to build the plot (grid cube) is shown. b) Same as a), but multiplying the ED by the sign of λ_2 . Molecular graphics in this and other figures were drawn with the software Diamond 3.2 h, Copyright 1997–2012 Crystal Impact GbR, Bonn Germany, by Klaus Brandenburg.

analogous plot for a pair of neighboring benzene molecules extracted from the crystal and for the full experimental ED in bulk benzene. The ED and RDG are plotted within a cubic volume enclosing just three C–H and two C–C bonds of one reference benzene molecule, while a second one is almost entirely contained within the cube (see inset in Figure 1a), so that some intermolecular contacts can take place. Apart from the low RDG values when $\rho(\mathbf{r}) > 1.8 \text{ e} \text{ \AA}^{-3}$, that is, for ED values typical of covalent bonds in benzene, four spikes (three of which, at the lowest ED values, are nearly superimposed; see below) also appear in the low-ED/low-RDG region of the plot. This is just the distinctive feature of non-covalent interactions,^[37] as, according to [Equation (1)], $s(\mathbf{r}) \rightarrow 0$ when $|\nabla\rho(\mathbf{r})| \rightarrow 0$. Therefore, analogously to what was found by Johnson et al. by applying the RDG approach to in vacuo molecular dimers, an NCI fingerprint is, not unexpectedly, similarly obtained by using multipole-derived EDs, that include the information polarisation due to the crystal field. In Figure 1b, the RDG is shown against $\rho(\mathbf{r}) \cdot \text{sign}(\lambda_2)$ to discriminate between the supposedly attractive and the so-called non-bonded interactions (see above). In this way, two out of the three spikes originally placed at lowest absolute ED values shift towards negative-signed ED values. They correspond to interactions associated with a (local) negative λ_2 curvature of $\rho(\mathbf{r})$ and are therefore somewhat attractive in nature. The remaining third spike has instead a positive and close-to-zero $\rho(\mathbf{r}) \cdot \text{sign}(\lambda_2)$ value, associated with the intermolecular ring

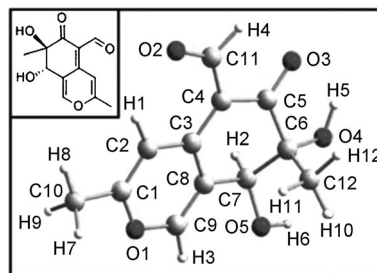
critical point (RCP). The spike at slightly higher ED value in Figure 1a is also moved to positive values in Figure 1b, since it marks the RCP at the centre of the second aromatic ring (the one relative to the reference molecule lies out of the volume considered).

The presence of an ED critical point ($\nabla\rho(\mathbf{r})=0$) is not strictly required for an RDG spike to appear in the ED/RDG plot. In other words, the RDG-based NCI descriptor is potentially able to single out not only stabilizing, pair-specific chemical bonds (those marked by atomic interaction lines in “classical” QTAIM), but also other, somewhat elusive, through-space interactions, not necessarily stabilizing nor implying the appearance of a bond path in the ED scalar field.

In summary, regions of space characterised by relatively low RDG values bear information on NCI that may be visualised by plotting “low-RDG” isosurfaces in these same regions. Selecting a reasonable RDG isovalue is usually not problematic; it is customarily set at more or less half of the highest RDG value of the points in the spikes observed in the RDG/ED plot. The only rule of thumb is that of using the same RDG value when different NCI isosurfaces are compared, either in the same or in different systems. This holds true whenever a single method was employed to obtain the related EDs. Otherwise, different RDG values may be required to compare on similar grounds the RDG-based results for differently derived ED (e.g. from wave function, multipole model, etc.).^[50] This is, however, a delicate and debatable assumption when contrasting the performance of “true” EDs with that of the independent atom model (IAM) ED.^[51] For true EDs, the main effect of different methods on the $s(\mathbf{r})$ versus $\rho(\mathbf{r})$ diagram is a shift of peaks; thus, in order to obtain comparable images just a shift of cut-offs is needed. This can be related to the fact that $s(\mathbf{r})$ roughly behaves like $\rho^{-1/3}$ (see Equation (3) in ref. [38]), so that the effect of the method on the density is directly followed by the RDG. In their seminal paper, Johnson et al. used RDG values between 0.4 and 0.7 for true EDs. In this work, but for a few indicated exceptions, we employed a single value of 0.4 for the *ab initio* and of 0.6 for the multipole-derived RDGs of all systems considered. More details on the adopted grid and cut-offs can be found in Supporting Information S4.

Another choice to be made concerns the signed-ED interval. If only NCI are to be examined, this quantity should be chosen so that the contribution from covalent bonds is excluded and a $\rho(\mathbf{r})\cdot\text{sign}(\lambda_2)$ value falling between the low-ED spikes and the region of low RDG at higher ED is recommended. The appropriate RDG isovalues and signed-ED intervals are selected by examining the ED/RDG plot case by case. In this work, for example, the admitted $\rho(\mathbf{r})\cdot\text{sign}(\lambda_2)$ range was always -0.05 a.u. (-0.337 e \AA^{-3}) $< \rho(\mathbf{r})\cdot\text{sign}(\lambda_2) < 0.05$ a.u. ($+0.337$ e \AA^{-3}). In Figures 2–9 the same colour scale was employed, ranging from -0.03 (red) to 0.035 (violet) a.u. Note that this colour code convention does not correspond to that used in refs. [37] and [38].

Austdiol: austdiol (Scheme 1) is a fungal metabolite whose crystal structure and charge density were deeply investigated by Destro et al.^[41,52] It crystallises in the unusual space



Scheme 1. Atom labels and chemical formula of the fungal metabolite austdiol. Molecular graphics in this and other schemes were drawn with the software Diamond 3.2h, Copyright 1997–2012 Crystal Impact GbR, Bonn Germany, Klaus Brandenburg.

group $P2_12_12$ as a consequence of the coexistence of two main packing patterns in the bulk. Indeed, within the *ab* plane the molecules are held together by relatively strong O–H...O hydrogen bonds (HBs) involving a hydroxyl, the keto and the aldehyde groups (Figure 2a).

Therefore, an overall zigzag ribbon^[53] HB pattern is generated along the *a* axis. At the same time, such a pattern forces each pair of molecules in the *ab* plane to be C_2 symmetry-related, and therefore excludes the possibility of a third 2_1 axis parallel to *c* existing. Rather, different molecular layers along *c* are connected by considerably weaker CH...O HBs. According to ref. [41], we considered as true HBs only those H...O contacts for which the Koch and Popelier criteria are satisfied.^[54] The isosurfaces relative to some of the relevant inter- and intramolecular X–H...O (X=C,O) contacts of austdiol are shown in Figures 2 and 3, respectively, while Table 1 reports their corresponding geometrical and topological features. Figure 4 displays isosurfaces relative to three weak C–H...O intermolecular interactions along *c*.

Intermolecular hydrogen bonds: Johnson et al. showed that relatively strong HBs, such as those formed in water and formic acid dimers, result in disc-shaped, contracted RDG isosurfaces with $\lambda_2 < 0$ curvatures.^[37] Figure 2b–d display the RDG surfaces computed from the experimental ED for the quite strong intermolecular H...O HBs in the *ab* plane of the unit cell of austdiol (Figure 2a). Some disc-shaped, negative-valued RDG isosurfaces are indeed recognizable (Figure 2b–d), together with more complex ones arising from the formation of cyclic H-bonded patterns due to the crystal packing. This is in particular the case for the H5...O3 interaction (Figure 2d), where a green-blue surface winds in the free space between two C_2 symmetry-related molecules. Indeed, the two facing O3 atoms are linked through a BP, and therefore produce an RDG isosurface containing the BCP, the two corresponding RCPs and even an intramolecular O4–H5...O3 contact per molecule (see below). The other

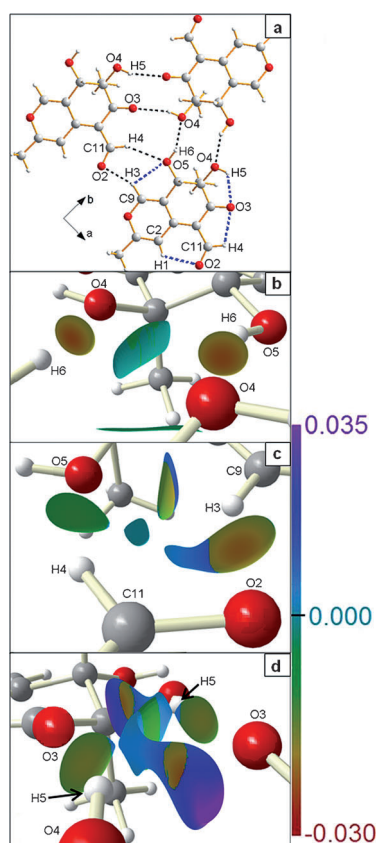


Figure 2. a) Inter- (black) and intramolecular (blue) hydrogen-bond network in the *ab* plane of austdiol. All of the interactions marked in this panel are shown as corresponding RDG isosurfaces in Figures 2 and 3. b–d) RDG-based NCI isosurfaces for X–H...O (X=C, O) contacts of austdiol. The color scale for $ED \cdot \text{sign} \lambda_2$ [$e \text{ au}^{-3}$] is shown on the right. The isosurfaces in this and the following figure were drawn with the software MolIso.^[81]

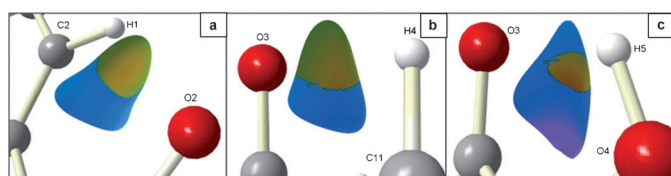


Figure 3. RDG-based NCI isosurfaces for selected X–H...O (X=C, O) intramolecular contacts of austdiol. See Figure 2 for the molecular geometry and the color legend.

important O–H...O bond is the H6...O4 one (Figure 2b). Again, the pair of symmetry-related HBs is characterised by disc-shaped, $\lambda_2 < 0$ surfaces. On the other hand, the third green surface visible between them is the signature of the ring critical point. At variance with the RCP-related surface within the benzene ring,^[37] it is quite elongated, possibly as a result of the much smaller symmetry in the ring in the present case and of the fact that the internuclear axes related to 1,4 (O4...O5) or higher “topological” non-bonded contacts (1,5: O5...O5, O4...O4, H6...H6) either do not intersect or do so at different points.

Table 1. Geometrical and topological features of some intermolecular and intramolecular X–H...O contacts (X=C, O) of austdiol.^[a,b]

Bond (Figure)	ρ_{BCP} [$e/\text{\AA}^3$]	$\nabla^2 \rho_{\text{BCP}}$ [$e/\text{\AA}^5$]	$d_{\text{H}\cdots\text{O}}$ [\AA]	X–H–O [$^\circ$]
Intermolecular				
O5–H6...O4 ^[c] (2b)	0.14(4)	1.34(6)	2.023	153.2
O4–H5...O3 ^[d] (2d)	0.09(4)	1.11(5)	2.114	158.4
C9–H3...O2 ^[e] (2c)	0.13(3)	1.40(4)	2.174	150.7
C11–H4...O5 ^[f] (2c)	0.05(2)	0.56(1)	2.519	154.1
C12–H11...O2 ^[g] (4b)	0.05(3)	0.83(2)	2.443	163.4
C10–H7...O3 ^[h] (4b)	0.04(3)	0.41(1)	2.544	166.9
C12–H11...O1 ^[h] (4b)	0.03(1)	0.33(<1)	2.979	116.9
Intramolecular				
C9–H3...O5 (2c)	no BCP	no BCP ^[i]	2.461	92.1
C2–H1...O2 (3a)	0.11(3)	2.00(3)	2.145	121.8
C11–H4...O3 (3b)	no BCP	no BCP ^[i]	2.359	100.5
O4–H5...O3 (3c, 2d)	no BCP	no BCP ^[i]	2.052	116.9

[a] The labels reported in parentheses in column 1 refer to the figures in which the corresponding RDG-based NCI isosurfaces are portrayed. [b] For electron and Laplacian densities, standard uncertainties (s.u.) are given in parentheses. The s.u. on the Laplacian are well known to be underestimated when using XD2006. The s.u. on the geometrical parameter cannot be correctly estimated, since the hydrogen positions were not refined; however, the s.u. on $d_{\text{H}\cdots\text{O}}$ should be on the order of 0.001, and those on the angle on the order of 0.1 (see ref. [41]). [c] At $-x, 1-y, z$. [d] At $1-x, 1-y, z$. [e] At $-1+x, y, z$. [f] At $1+x, y, z$. [g] At $-0.5+x, 0.5-y, -z$. [h] At $0.5+x, 0.5-y, -z$. [i] $\lambda_2 < 0$ at the midpoint of the H...O vector.

The C9–H3...O2 contact is worthy of separate discussion (Figure 2c), as it is quite short (Table 1) and it was estimated to have strength comparable to that of the above described OH...O bonds.^[41] Such evidence is recovered in the NCI framework: the corresponding signed isosurface, and in particular its negative part, looks similar to those discussed above for the OH...O HBs, even though it is not as disc-shaped because of the presence of a non-bonded contact involving C11 and H3 atoms in symmetry-related molecules.

Intramolecular hydrogen bonds: For the intramolecular H...O contacts, which are certainly important in determining the molecular conformation observed in the bulk, a BP was found only for the C2–H1...O2 interaction. On the contrary, a RDG isosurface depicts each of the six unique intramolecular H...O contacts, no matter whether a BP is present or not (three isosurfaces for non-bonded contacts are shown in Figures 3b,c and 2c). Interestingly, the RDG isosurface of the C2–H1...O2 HB (Figure 3a) is characterised by two well-defined regions of positive and negative λ_2 , respectively, due to the presence of an RCP near (0.61 \AA away) the HB BCP. This was expected on the basis of the ED topology in a ring when a bond is significantly weaker than the others.^[25] Note, however, that RDG isosurfaces provide a similar picture also for the remaining non-bonded intramolecular C–H...O contacts, including those in Figures 3b and 2c. In general, the farther the hydrogen atom is from the oxygen atom, the more the CHO angle is bent and the smaller the $\lambda_2 < 0$ zone on the isosurface. However, such a trend is not neat and not always respected. The simultaneous involvement of the H and of the acceptor O atoms also in significant intermolecular interactions (this is the case for

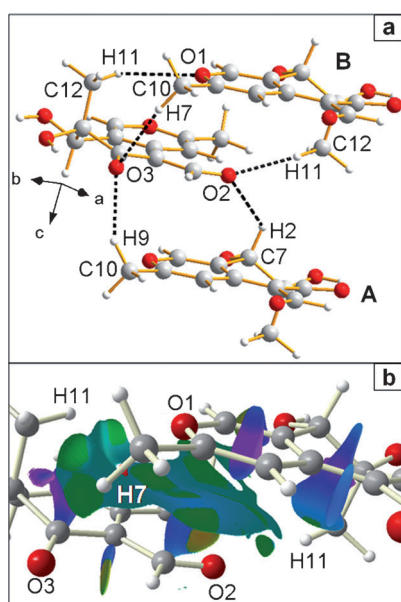


Figure 4. RDG representation of NCI for austdiol along the *c* axis. See Table 1 for the symmetry operations relating the showed molecules. a) Crystal packing along the *c* direction. b) RDG-based NCI isosurfaces for the B molecular pair, formed by the central molecule and the upper one in a).

H4, H5, H6, O2, O3, O4, O5 in austdiol) may complicate the picture and affects the shape and the relative fractions of positive- and negative-signed RDG isosurfaces for the intramolecular interactions besides what is expected on the basis of the geometry of the intramolecular CH...O interaction alone. This external perturbation is particularly evident in the case of the two intramolecular O–H...O non-bonded contacts. For instance, the O4–H5...O3 interaction (Table 1 and Figure 3c) shows a larger isosurface, almost completely characterised by positive λ_2 . The H5 atom is also contemporarily involved in a strong, almost linear, intermolecular O–H...O contact with the same type of O atom (O3) but belonging to another molecule (Table 1). Interestingly, the O4–H5...O3 contact forms a BP in the gas-phase, that is, when no intermolecular interactions compete for stronger HBs. In this context, the RDG-based NCI descriptor may be useful to highlight the environment effects on the relative strength and nature of such contacts.

Van der Waals interactions: Proper modelling of van der Waals and, in particular, dispersion interactions is known to be difficult both in vacuo^[55] and in molecular crystals.^[11b,24,56] These interactions are due to time-dependent perturbations of the ED and imply correlations among distant electrons. Therefore, they cannot be correctly taken into account by ground-state adiabatic methods, such as standard DFT theory, wherein the exchange-correlation potential is estimated on the basis of a finite number of the static ED derivatives.^[55,57] Moreover, dispersion interactions are inherently non-local in nature, as they correlate the overall charge density distributions of individual molecular moieties to each

other.^[58] Even though dispersion forces do not significantly affect ED,^[59] they play an important role in lowering the overall interaction energy of the system.^[24] The ability of the NCI descriptor to highlight subtle intra- and intermolecular density features typically associated with dispersion interactions was discussed in detail in ref. [37]. Indeed, in complexes like methane dimer, large and almost flat isosurfaces appeared in regions characterised by very low and almost constant ED values.^[37] It was also demonstrated there that MP2/6-311++G** calculations produce virtually identical NCI isosurfaces to B3LYP/6-31G* ones, despite the different interaction-energy estimates of these two methods.^[37]

For the experimental ED of austdiol, quite large RDG isosurfaces were found for the two unique neighbouring molecular pairs along the *c* direction (structure in Figure 4a; signed RDG isosurfaces are shown in Figure 4b and only for the molecular pair labelled as B in Figure 4a). Three C–H...O bonded contacts, based on the BP criterion, hold together the molecular pair in Figure 4b. Two such contacts (i.e., C12–H11...O1 and C10–H7...O3) are very weak, and the former was even found^[41] not to satisfy the Koch and Popelier criteria^[54] for hydrogen bonding. Indeed, they are not recognizable through specific RDG isosurfaces. Rather, a single, broad van der Waals-like isosurface has merged with and encompasses the two slightly negative, diffuse and non-disc-shaped regions around the BCPs of the two interactions. This behaviour may be explained in terms of the marginal difference between a closed-shell dispersive interaction and an extremely weak and long C–H...O bond. Moreover, the ED is relatively flat in this region. Therefore, the λ_2 eigenvalue is always very close to zero and its sign turns out to be quite indeterminate. This implies that both positive and negative values are present when the $\rho(\mathbf{r})\text{sign}(\lambda_2)$ quantity is mapped onto the RDG isosurface. Similar conclusions apply to the corresponding theoretically derived NCI isosurfaces for both RDG=0.4 and 0.6 isovalues (see Supporting Information Figure S5.3). Figure 4b also displays a clearly recognizable disc-shaped RDG isosurface for the C12–H11...O2 intermolecular hydrogen bond that connects neighbouring molecules outside the *ab* plane (i.e., at different heights along *c*). Actually, in this case, besides the comparatively short H-bond length (Table 1), the H...O direction is almost parallel to the molecular layers in the *ab* plane and the HB takes place in a region where the non-directional purely steric-dispersive interactions do not play the dominant role.

In general, the electronic excitations causing dispersive interactions are always present, but the characteristic large and flat RDG isosurfaces associated with such interactions emerge only if stronger interactions (e.g., OH...O, but also strong CH...O hydrogen bonds) are not simultaneously active within the same region of space. Moreover, strictly speaking, purely dispersive, van der Waals interactions are always *attractive*. Yet, in Figure 4b the $\text{sign}(\lambda_2)$ quantity is positive throughout vast areas of the RDG isosurfaces. According to the interpretation of the NCI descriptor,^[37] this indicates that (several) atoms are in “nonbonded” contact

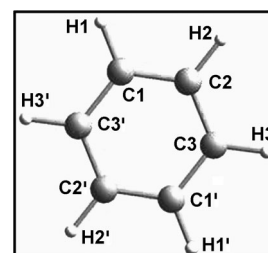
(closed-shell interactions), but, clearly, it does not also imply that the overall interaction revealed by the RDG isosurface is destabilizing. Note that the NCI descriptor explores the behaviour of the RDG in a specific region, whereas the interaction energy is the result of a balance involving forces which effectively operate in a larger portion of space. Moreover, the observed crystal packing is the outcome of a subtle competition among different energy contributions, and there is always a certain degree of arbitrariness in partitioning the overall cohesive energy of a crystal into “stabilizing” and “repulsive” terms.^[60] As reminded by Bader,^[25,61,62] there are no net attractive or repulsive forces acting on a field-free quantum system at the equilibrium, as in that case the overall balance of the quantum mechanical Eherenfest and Feynman forces (acting respectively on electrons and nuclei) is exactly zero. In conclusion, the so-called van der Waals-like large and flat RDG isosurfaces described above should be considered as tools to highlight those regions of space characterised by steric crowding and dispersive interaction balance, rather than as a way to “see” or “localise” van der Waals dispersive interactions in the bulk, which by their very nature are neither local nor static. Another word of warning concerns the soundness of the energy classifications proposed for the signed RDG isosurfaces^[37] when they enclose regions of flat and low X-ray-derived EDs, particularly prone to both random and systematic experimental errors.

RDG isosurface shape versus NCI type and the adopted electron density model: From the results presented here for austdiol, it emerges that a one-to-one inverse correlation seems to exist among the directionality (and the strength) of specific non-covalent interactions and the surface/volume ratio of the corresponding RDG isosurface. In particular, the stronger the NCI, the smaller and more disc-shaped the RDG surface appears in real space, and at the same time is characterised by more negative $\rho(\mathbf{r})\text{-sign}(\lambda_2)$ values (see also refs. [37] and [38]).

Concerning the effect of the choice of the ED model, we found that the results described above for the various types of interactions using the experimentally-derived ED satisfactorily agree, on average, with those obtained from the fully periodic wavefunction of austdiol (see a full comparison of the experimental and theoretically derived RDG isosurfaces in Supporting Information S5). However, even if the HB strength hierarchy is predicted to be the same by the two model EDs, a few significant differences emerge, namely, a slightly different shape of the RDG isosurface of the H1...O2 intramolecular interaction and apparent “strengthening” of the weakest intermolecular HBs reported in Table 1 on passing from experiment to theory (e.g., see the H1...O2 and H7...O3 interactions in Supporting Information Figures S5.2 and S5.3 and the discussion thereof). These differences are not unique to the RDG-based NCI descriptor, but are already manifest in the ED values at BCPs (Supporting Information Table S5.1). A slight disagreement between the experimental and theoretical RDG-derived NCI description is anticipated, since the difference

$\rho(\mathbf{r})_{\text{periodic,theo}} - \rho(\mathbf{r})_{\text{multipole,expt}}$ is clearly not constant for each point \mathbf{r} and it is likely to be greater, on percentage, when small $\rho(\mathbf{r})$ values are considered (see above). As a consequence, in some cases use of a different RDG isovalue for different interaction types is required to fully match theoretical and experimental results. Moreover, the $\text{sign}(\lambda_2)$ quantity may be basically indeterminate in regions characterised by flat ED, as it may subtly depend on the choice of the Hamiltonian and basis set (as concerns theory) or on the overall quality of the multipole ED (as concerns experiment). Therefore, besides the interpretive warnings pointed out before, great care should be employed in assigning an attractive or repulsive nature to interactions characterised by a RDG isosurface with low- $|\lambda_2|$ value.

Benzene: Benzene (Scheme 2) is the prototypical system for studying aromaticity and, in general, π -electron-mediated NCI. It crystallises, below 270 K, in the centrosymmetric *Pbca* space group, with half a molecule in the asymmetric unit and four molecules or, equivalently, four unique pairs of molecules in the unit cell. The crystal packing of aromatic and polyaromatic compounds was largely investigated by Desiraju and Gavezzotti,^[63] who classify the typical packing motif in crystalline benzene as a herringbone structure, which was found to maximise the number of C–H... π and C–H...C interactions, and this feature is clearly reflected by the NCI descriptor (see below).



Scheme 2. Atom labels for benzene. Primes refer to inversion-related atoms.

Table 2 reports the topological properties of the ED BCPs found for each unique molecular pair, and Figures 5 and 6 show the corresponding RDG isosurfaces for the pair I and pairs II–IV, respectively. For pair I, NCI isosurfaces (Figure 5a) are associated with two intermolecular bond paths (Figure 5b).

Table 2. Geometrical and topological (BCP) data for intermolecular C–H...C and C–H...H interactions in the benzene crystal.^[a,b]

Bond (Figure)	ρ [$e/\text{\AA}^3$]	$\nabla^2\rho$ [$e/\text{\AA}^3$]	$d_{\text{H}\cdots\text{C}}$ [\AA]
C3...H2 ^[c] (5a)	0.030(4)	0.256(1)	3.065
C1...H3 ^[c] (5a)	0.042(6)	0.371(2)	2.862
C1...H3 ^[d] (6a)	0.016(5)	0.235(1)	2.955
H2...H1 ^[e] (6a)	0.018(4)	0.275(1)	2.638
H3...H2 ^[f] (6b)	0.013(5)	0.238(1)	2.548
C3...H1 ^[f] (6b)	0.024(4)	0.241(1)	2.934
C3...C2 ^[g] (6c)	0.001(<1)	0.008(<1)	5.295

[a] The labels reported in parentheses in column 1 refer to the figures in which the corresponding RDG-based NCI isosurfaces are portrayed. [b] Electron and Laplacian density values s.u. are given in parentheses. [c] At $-0.5-x, -y, -0.5+z$. [d] At $-x, 0.5+y, 0.5-z$. [e] At $+x, 0.5-y, 0.5+z$. [f] At $-0.5-x, -0.5+y, +z$. [g] At $-1-x, -y, -z$. The BCP was recovered by using only the multipoles of the two molecules (see text).

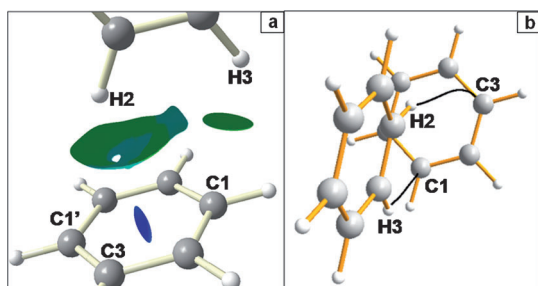


Figure 5. a) RDG-based NCI isosurfaces for the molecular pair I in the benzene crystal. b) Intermolecular bond paths for the same molecular pair. See Figure 2 for color legend.

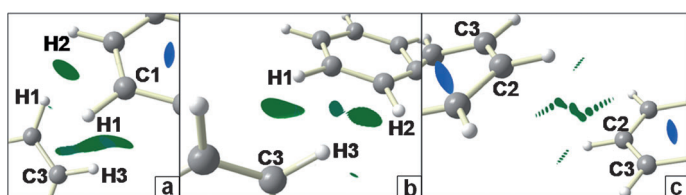


Figure 6. RDG isosurfaces for molecular pairs II (a), III (b) and IV (c) in the benzene crystal. a) Contacts H1...H2, C1...H3. b) Contacts H3...H2, C3...H1. c) C3...C2. See Figure 2 for the colour legend and Table 2 for the symmetry operations.

These two BPs link C3 and C1 with H2 and H3 at $-0.5-x$, $-y$, $-0.5+z$. From the QTAIM perspective, this should indicate two well-defined CH...C interactions. However, the H2...C3 BP is significantly bent, because the BP points towards the (3, -1) critical point of the C3–C1' covalent bond and then suddenly deviates towards the (3, -3) nuclear C3 attractor (Figure 5b). Moreover, the H2 atom is roughly equidistant from all the carbon atoms belonging to the other molecule of the pair, as the $d_{H...C}$ distances range from 3.065 Å (H2...C3) to 3.109 Å (H2...C1). All of these features, typical of systems showing CH... π interactions,^[64] suggest that H2 should in fact similarly interact with all the carbon atoms of the symmetry-related molecule, giving rise to a C–H... π attractive contact involving the whole π -electron cloud of the facing aromatic ring. Indeed, the RDG-based NCI descriptor (Figure 5a) gives rise to a large doughnut-like isosurface that, from the viewpoint of the H2 hydrogen atom, covers almost entirely the hydrocarbon ring of the other molecule. This picture clearly clashes with that provided by the BP analysis, which favours interaction of the H atom with just one single atom of the ring.^[65] However, the $\rho(\mathbf{r})\text{-sign}(\lambda_2)$ quantity is slightly more negative (light green zone of the surface in Figure 5a) between H2 and its nearest carbon atom (C3), and thus somewhat mirrors the presence of the BP connecting these two specific atoms. The RDG isosurface looks to some extent similar to the broad surfaces that are associated with the steric/dispersive interactions in austdiol (see above); in fact, C–H... π interactions are essentially dispersive in nature.^[64] Nonetheless, the surfaces associated to CH... π and “pure” van der Waals-like interactions differ in that the former appear more localised in

space, owing to their clear association to the dispersive interactions arising from the π system.

The signed RDG isosurface of the other CH...C interaction (H3...C1) appears instead much smaller, disc-shaped and only slightly negative. All of these features comply with a conventional, very weak HB, as anticipated by the largely unsymmetrical location of H3 with respect to the ring atoms of the other molecule in the pair and by the almost straight BP and density properties at the BCP. The RDG-based NCI and BP pictures nicely match in this case.

In both molecular pairs II and III (Figure 6a and b) two similar BPs are present. One links an H to a C atom (CH...C contact), whereas the other connects two H atoms. The shape of the RDG isosurface associated to the first BP for the molecular pair III resembles those found for intermolecular HBs in austdiol (see above) and in benzene pair I, although in this case it appears slightly broader in space, while the isosurface relating to the same contact in molecular pair II is definitely more elongated. This shape could likely be the result of C1–H1 and C3–H3 bonds facing each other. Nearly disc shaped isosurfaces were found also for the H...H contacts. In general, all the surfaces associated with H...C and H...H contacts in Figure 6a and b are relatively broad and have signed $\rho(\mathbf{r})$ values quite close to zero, albeit negative. In other words, they signal weakly attractive interactions, only partly localised between the atom pairs that give rise to the QTAIM BPs. The appearance of the isosurfaces is somewhat intermediate between the van der Waals-like and HB ones, as it could reasonably be inferred on the basis that weakly dispersive interactions should play a significant role in almost apolar H...C and H...H contacts.^[66]

The CH...C interactions in Figure 6a and b (see also the theoretically derived ones in Supporting Information Figure S5.4) are formally equivalent to a very, very weak HB, as they follow the trend sketched above on going from relatively strong (OH...O) to weak (CH...O) HB interactions (see above). Nevertheless, RDG isosurfaces and BPs depend to some extent on the whole set of interactions present in a system. In the case of the BP this may, for instance, be revealed by the Source Function contributions of the various atoms to the ED at each point of the BP.^[35] Analogously, the smaller or larger size of the RDG isosurfaces provides an insight on the more or less local character of an interaction, respectively. It is thus not granted that the broad, dark green surfaces between H and C in Figure 6a and b are exclusively due to the interaction between the two facing atoms.

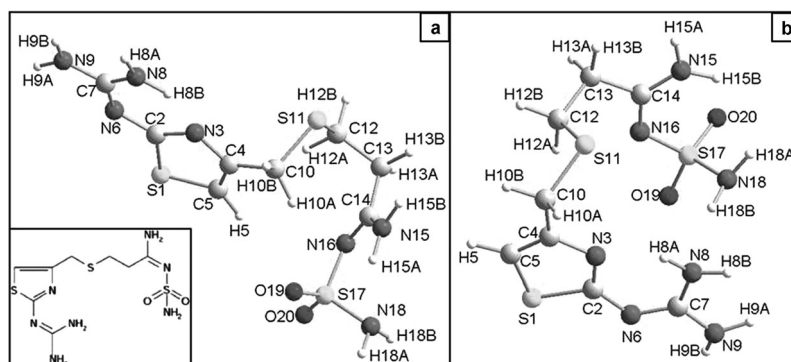
Molecular pair IV (Figure 6c) deserves specific comments. In such a pair, the centres of mass of the two molecules are 6.78 Å apart (see also Table 2). When the multipole ED for this pair extracted from the crystal is considered, two intermolecular C...C BPs are found between the C2 atom of the reference molecule and the C3 atom at $-x$, $-y$, $1-z$, and vice versa. The corresponding BCPs have a very low ED (Table 2). In the RDG-based approach, a broad and low-ED isosurface appears, which therefore represents some kind of

very weak, albeit attractive interaction (based on the λ_2 sign). The latter could be interpreted as a sort of dispersion-driven $\pi\cdots\pi$ interaction among the lateral C atoms of the two molecules. However, when also the multipoles of the neighbouring molecules are considered, that is, when the same analysis is performed in the bulk, both the BPs and the RDG isosurfaces disappear. This implies that the $\Delta\rho$ term [Eq. (2)] is no longer negligible and follows from the fact that the two molecules are

quite far apart from each other. Actually, in this case the relative contribution to ED in the intermolecular region due to other molecules in the unit cell increases at the expense of that due to the multipoles belonging to pair IV. In particular, when the multipoles associated with the $\Delta\rho$ term are considered, the quantity $|\nabla\rho(\mathbf{r})|$ in Equation (1) increases more than the ED itself, and the RDG values rise well above the value used for defining the RDG isosurface.^[67] A possible explanation of this behaviour may be that, even though a very weak $\pi\cdots\pi$ interaction may take place in pair IV, it is negligible with respect to other stronger interactions (CH $\cdots\pi$, dispersive) present in the benzene crystal. Interestingly, similar RDG isosurfaces appear when they are computed on a quantum mechanical ED of an isolated benzene molecular pair at the same crystal geometry, whereas they are no longer present when the fully periodical ED is considered (see Supporting Information Figure S5.4). All of this agrees with the conclusions drawn above for austdiol with regard to the conditions which are required to make the RDG isosurfaces related to van der Waals interactions visible and even with literature findings.^[63] At the same time, what we found provides evidence that the NCI features displayed in Figure 6c are likely not due to artefacts of the multipole model.

Famotidine: Famotidine (Scheme 3) is an heteroatom-rich anti-ulcer drug. Two different polymorphs of this compound are known^[68] to date ($P2_1/c$ and $P2_1/n$), which differ from each other in both their crystal packing and molecular conformation. Form A, which is the thermodynamically stable one, adopts an “elongated” conformation, while the kinetically favoured modification B has a folded “hairpin” geometry. Most of the intermolecular interactions in both polymorphs are similar to the HBs and van der Waals-like contacts that were discussed above for austdiol and benzene. In this section, therefore, we mainly focus on the NCI results regarding interaction types not yet analysed, that is NH \cdots N HBs and other relevant interactions involving π electrons or sulfur atoms.

Both the A and B polymorphs show an intramolecular N-H \cdots N BP between a guanidinic NH $_2$ group as H donor and



Scheme 3. a) Molecular conformation of polymorph A of famotidine. b) Molecular conformation of polymorph B. Bottom left inset: chemical formula of famotidine.

the thiazole N atom as H acceptor. The topological features of the BCP indicate that this HB is the strongest among all hydrogen bonds considered so far. In fact, it may be classified as a resonance-assisted HB.^[69] Interestingly, the topological descriptors for this interaction are different on going from the form A to form B (see Table 3). In particular, this HB is significantly stronger in polymorph B, as the H \cdots N distance undergoes a shortening of about 4 % and the ED at the BCP increases by about 28 % (see Table 3). In general,

Table 3. Geometrical and BCP properties of the intramolecular N-H \cdots N interaction for the two polymorphs A and B of famotidine.

	A	B
	H8B \cdots N3	H8A \cdots N3
ρ [$e \text{ \AA}^{-3}$]	0.18(2)	0.23(3)
$\nabla^2\rho$ [$e \text{ \AA}^{-5}$]	3.52(4)	3.62(5)
$d_{\text{H}\cdots\text{N}}$ [\AA]	1.928	1.853
N-H-N [$^\circ$]	130.6	131.2
λ_1	-0.99	-1.19
λ_2	-0.59	-0.93
λ_3	5.09	5.74
$d_{\text{BCP-RCP}}$ [\AA] ^[a]	0.839	0.830

[a] Distance from BCP to the nearest RCP.

from the QTAIM perspective, strong (but still mainly electrostatic) HBs show a larger contraction of ED towards the BP and from the BCP towards the nuclei with respect to weaker ones. This is reflected in higher negative values for the λ_1 and λ_2 density curvatures (related to the directions of maximal charge decrease perpendicular to the BP at BCP) and in higher positive value for the λ_3 curvature along the BP at BCP, as is indeed the case for the interaction considered here.^[42]

The RDG isosurfaces for this NH \cdots N interaction in both polymorphs are shown in Figure 7. In this case the shape of the region with negative λ_2 value is more disc-like and contracted in space with respect to those found for the intramolecular HBs in austdiol (see above). This effect is particularly evident for the B form, when compared to that for the A form (Figure 7). As discussed above, these features correlate with the HB strength, and again the QTAIM and RDG sce-

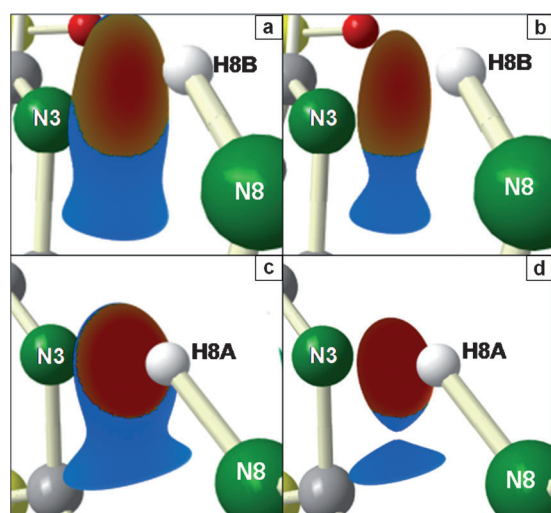


Figure 7. N–H...N intramolecular H-bonds in famotidine. See Figure 2 for the signed ρ colour legend. a) Polymorph A, reduced density gradient $s(\mathbf{r})=0.6$. b) Polymorph A, $s(\mathbf{r})=0.45$. c) Polymorph B, $s(\mathbf{r})=0.6$. d) Polymorph B, $s(\mathbf{r})=0.45$.

narios mutually support each other. The ED contraction commented on above is larger in the B form, and the $|\nabla\rho(\mathbf{r})|/\rho(\mathbf{r})^{4/3}$ ratio, due to the larger λ_i ($i=1-3$) magnitudes (especially λ_2), changes more rapidly, and thus yields smaller RDG isovalue domains in such form. This can be in fact be seen also from the smaller negative- λ_2 region found in polymorph B. The contraction of the RDG surface as a function of HB strength becomes even clearer if the RDG isovalue is diminished from 0.6 to 0.45 (Figure 7d). Reducing such a value may result in a splitting of the original RDG domain of higher isosurface value into sub-domains. This is typically the case when the original domain encompasses more than one critical point in the density. At a given lower RDG value, the RDG domains associated with the two critical points will start to separate. The process is reminiscent of the electron localisation function (ELF) analysis wherein, by continuously increasing the ELF isovalue from 0 to 1, the initial reducible basin containing all three-dimensional attractors of a given system progressively splits up into its component irreducible domains, each of which contains just one ELF local maximum.^[70] Diminishing the RDG isovalue to 0.45 yields a splitting of the original RDG=0.60 isosurface domain into two sub-domains only in polymorph B, one of which is related to the BCP and the other to the RCP. Concerning the fully periodic ED, the RDG=0.6 and 0.45 domains look both very similar to those obtained from the multipole ED, and this holds true for both the polymorphs (see Supporting Information Figure S5.7). In the present case, given the relatively strong character of the analysed HB interaction, no scaling of the RDG isovalue was required to match almost perfectly the theoretical and experimentally derived surfaces (see discussion above).

Figure 8a shows a CH... π -type intermolecular interaction similar to those found in benzene for polymorph A. In this case, however, only a single bond, namely, N6–C2, conjugat-

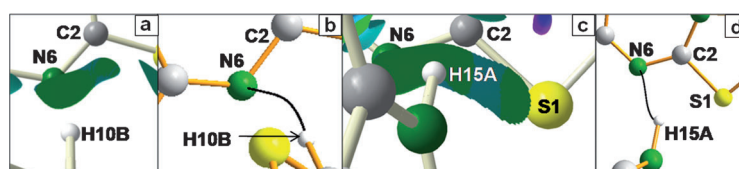


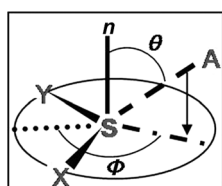
Figure 8. RDG-based NCI isosurfaces and bond paths for two intermolecular H-bonds of famotidine (polymorph A). See Figure 2 for the color legend. a, b) C–H... π interaction involving the N=C bond at $1-x, 0.5+y, 1.5-z$ and the corresponding H10B...N6 bond path, c, d) Same as a, b), for the interaction between H15 and the atoms N6, C2 and S1 at $x, 0.5-y, 0.5+z$. Only the H15A...N6 bond path is observed.

ed with the thiazole system, acts as acceptor in the CH... π contact. In other words, this CH... π interaction appears to be more localised with respect to those involving the entire aromatic ring in benzene (see above). In any case, both the QTAIM and the NCI descriptor approaches provide evidence for the existence of such an interaction. Regarding QTAIM, the BP relating H10B and N6 atoms points towards the covalent N6–C2 BCP and then deviates to reach the N6 attractor (Figure 8b). The NCI descriptor, on the other hand, shows a typical low-ED RDG isosurface between the hydrogen atom and the conjugated bond. Interestingly, at variance with similar surfaces detected for benzene, that shown in Figure 8a is relatively constricted in space, as it does not extend far away from the N6–C2 bond. However, the ab initio derived picture, at least at the adopted level of theory (see Computational Section), significantly disagrees with the multipole one, no matter the RDG value chosen to build up the isosurfaces. In more detail, the ab initio ED in the bulk exhibits a more disc-shaped RDG isosurface, deformed in such a way as to suggest a preferential interaction of H10B with the π cloud of the N6–C7 rather than that of the N6–C2 bond (see Supporting Information Figure S5.5). Indeed, at variance with what suggested by the formal bonding scheme shown in Scheme 3, the N6–C2 bond is much shorter (1.355 Å) than the neutron-estimated^[71] value for a single bond (1.488 Å) and slightly longer than both the neighbouring N6–C7 bond (1.339 Å) and the neutron estimate for an N–C double bond (1.336 Å). Both N–C bonds are thus significantly and similarly in conjugation with the thiazole system and may potentially act as π acceptors in CH... π interactions. The multipole-derived RDG features could thus be an artefact due to a failure of the multipole model, perhaps ascribable to subtle systematic errors/statistical noise affecting the experimental structure factor amplitudes. Yet, they could also point to inadequacies of the DFT functional that hamper a truly accurate description of low-ED regions of the theoretical charge density in this system. Certainly, such discrepancy deserves further investigation in the future.

An NH... π interaction is found in another molecular pair of the same polymorph A (see Figure 8c). The QTAIM picture clearly indicates an HB between H15A and N6, with an almost straight BP connecting the two atoms (see Figure 8d). The NCI descriptor, instead, suggests a more delo-

calised, through-space interaction somewhat relating the H15A atom with both S1–C2 and C2–N6 bonds. In this case, the RDG isosurface probably bears contributions arising from different interaction types. Therefore, it is difficult to disentangle the contribution due to the NH...N HB evidenced by QTAIM from other, less localised and somewhat more elusive interactions. The theoretically derived RDG isosurfaces for these interactions (see Supporting Information Figure S5.5) are anyhow markedly similar to those obtained from the multipole ED. In the present example, the joint RDG-NCI and QTAIM approach is more informative with respect to either of the two, as at least two different interaction types (NH...N HB and a possible NH... π interaction), coexisting in the same region of space, can be distinguished.

Non-covalent interactions involving S atoms have been studied for a long time, as, due to its large van der Waals radius and relatively high polarizability, sulfur is able to set up several interactions with its local environment in organic crystals (e.g., see ref. [72]).



Scheme 4. Geometrical parameters for the S...A contact. X and Y are the atoms covalently bonded to the S atom. θ is the angle between the normal \mathbf{n} to the YSX plane and the interacting atom A. Φ is the angle between the projection of the vector SA onto such plane and the line bisecting the YSX angle.

In 1977, Rosenfield et al.^[10] systematically investigated the geometrical preferences of the non-covalent contacts involving divalent S atoms and within the sum of the van der Waals radii of the interacting chemical species. In particular, they considered the polar coordinates θ and Φ with respect to the vector normal to the X-S-Y plane (Scheme 4) as possible approaching angles.

They concluded that $\theta < 40^\circ$ for the electrophilic species, whereas the nucleophilic ones approach S with $60^\circ \leq \theta \leq 90^\circ$ and $110^\circ \leq \Phi \leq 140^\circ$ (i.e., the nucleophile tends to lie almost in the X-S-Y plane, and preferably along the X–S or Y–S direction). In famotidine, only the former type of contacts is relevant, with hydrogen acting as the electrophilic species. The corresponding RDG isosurfaces for forms A and B are reported in Figure 9a,b and c,d, respectively (S1–H13A is not shown).

Nevertheless, as S atoms may behave either as nucleophiles or electrophiles, they can set up NCI in a key-lock mechanism even with other sulfur atoms. Figure 9b and d show contacts of this type in polymorphs A and B, respectively. In form A, S11 is linked through BPs to both H5 and S1, and therefore gives rise to a unique, broad isosurface characterised by $\rho(\mathbf{r})\text{-sign}(\lambda_2)$ close to zero and that contains the two BCPs and the RCP. Interestingly, however, the signed surface is negative in the regions between S11 and H5, and S1 and S11 (Figure 9b), that is, where the S...H and S...S contacts are likely to be attractive. By reducing the RDG

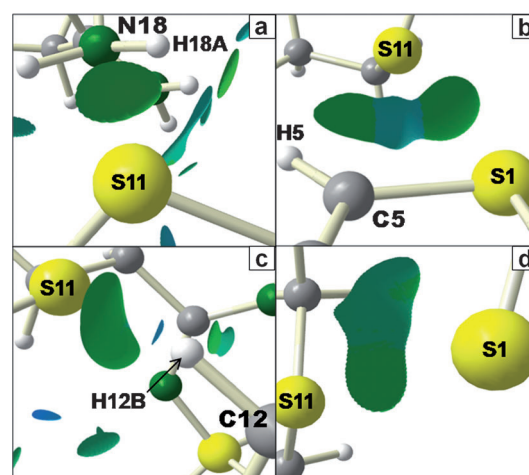


Figure 9. RDG-based NCI surfaces for intermolecular interactions involving S atoms in famotidine polymorphs A (a–b) and B (c–d). See Figure 2 for the colour legend and Table 4 for the labelling of the interactions here shown in the various panels.

isovalue, this NCI isosurface domain will necessarily split into three separate small domains, each associated with a critical point and with the two related BCPs likely bearing only a negative $\rho(\mathbf{r})\text{-sign}(\lambda_2)$ value on their isosurfaces.

In the QTAIM picture, all of the intermolecular contacts above described give rise to BPs, whose topological features are reported in Table 4 together with the θ and Φ parameters^[10] When S...H contacts are taken into account, the smaller the θ angle, the higher is the ED at the BCP and, therefore the stronger the bond. Interestingly, on passing from weaker to stronger S...H. interactions, the shape of the RDG isosurface changes from van der Waals-like (broad in space and sometimes with zones exhibiting both $\lambda_2 > 0$ and $\lambda_2 < 0$, Figure 9b and c) to HB-like (disc-shaped, $\lambda_2 < 0$, Figure 9a).

The same considerations hold true also for the S...S contacts. Indeed, in form A, S11 lies in the ideal “nucleophilic position” with respect to S1 ($\theta = 82.3$, $\Phi = 125.6^\circ$; Table 4). On the contrary, in form B, the θ angle is below (47.8°) and the Φ angle (154.0°) slightly above the 60–90 and 110–140° ranges retrieved in classical nucleophilic approach to the reference S atom. The RDG isosurfaces mirror these ar-

Table 4. Intermolecular BCPs involving sulphur atoms in famotidine.

Bond (polymorph, Figure) ^[a]	ρ [$e \text{ \AA}^{-3}$]	$\nabla^2 \rho$ [$e \text{ \AA}^{-5}$]	θ ^[b] [°]	Φ ^[b] [°]
S1...H13A ^[c] (A)	0.031(1)	0.514(4)	42.7	116.5
H18A...S11 ^[d] (A, 9a)	0.047(8)	0.603(4)	3.4	89.4
S1...S11 ^[e] (A, 9b)	0.031(2)	0.359(2)	(82.3/71.1) ^[h]	(125.6/162.0) ^[h]
H5...S11 ^[e] (A, 9b)	0.024(5)	0.306(2)	70.1	177.5
S11...H12B ^[f] (B, 9c)	0.019(1)	0.332(6)	74.9	119.8
S1...S11 ^[g] (B, 9d)	0.008(<1)	0.115(<1)	(47.8/70.2) ^[h]	(154.0/156.2) ^[h]

[a] Labels in parentheses refer to the polymorph, form A or B, in which the contact was found and to the figure in which the corresponding RDG isosurface is shown. [b] Angles are defined in Scheme 4. [c] At $-x, 0.5+y, 1.5-z$. [d] At $x, 0.5-y, 0.5+z$. [e] At $x, 1+y, z$. [f] At $x, 1+y, z$. [g] At $0.5+x, 0.5-y, 0.5+z$. [h] For the S...S contact the first (second) entry refers to the polar coordinates (reference system in Scheme 4) of the first (second) atom listed in column 1.

rangements, since the S...S contact gives rise to a disc-shaped negative surface in polymorph A, whereas in form B the analogous RDG surface appears definitely more spread in space. In any case, the agreement between the experimentally and theoretically derived pictures is excellent for this kind of NCI (see Supporting Information Figure S5.6).

In conclusion, this last test case confirms that the stronger the NCI, the smaller the surface/volume ratio of the RDG isosurface (and the most negative the signed ED mapped on it). Therefore, such a ratio could be taken as a qualitative criterion to rank on a relative (energy) scale interactions between the same kind of atoms (but in different environments and with different geometries) or, to some extent, also interactions between different atomic pairs in various chemical and structural situations.

Conclusion

We have applied for the first time the novel RDG-based NCI descriptor to multipole electron densities derived from single-crystal X-ray diffraction experiments at low temperature ($T \leq 100$ K). We have demonstrated that the experimentally derived multipole NCI picture is reliable and of comparable quality to that obtainable from a fully periodic ab initio approach. On average, we found a good agreement between experiment and theory, with the only exception of one C-H... π interaction in famotidine.

We have also explored in detail to what extent the RDG-based NCI descriptor provides a complementary picture to that offered by QTAIM. In the latter, the presence of a BP unequivocally highlights a stabilizing interaction, as the ED is homeomorphic with respect to the corresponding virial field.^[73] However, this picture is quite often too localised and unavoidably discontinuous (yes/no). Quite recently, it was proposed^[30] that the presence of a BP essentially signals privileged exchange path channels among topological atoms. Instead, the NCI descriptor, analogously to other continuous descriptors like the localisation/delocalisation indices or the Source Function, is able to visibly reflect the simultaneous occurrence of competing exchange path channels, rather than to single out just one or (in some special cases) a few dominant channels for electron exchange. For instance, the RDG descriptor depicts the case of inherently delocalised interactions (e.g., C-H... π interactions in benzene) in terms of extended, largely flat $s(\mathbf{r})$ isosurfaces, in contrast to the bond path analysis, which provides instead a fairly localised description of such an interaction. However, when the RDG isosurface domain contains more than one critical point in the electron density, the RDG-NCI and QTAIM pictures can be brought to a closer correspondence by progressively lowering the s isovalue, until the original RDG domain splits into its irreducible components. The hierarchy of the sequential splitting, along with the RDG value(s) at which such splitting occurs, brings further precious insight. Even more interesting are those cases where the QTAIM predicts a localised interaction, while the corresponding RDG isosur-

face remains fairly broad and apparently related to more than one atomic pair interaction, regardless of the chosen RDG isovalue. In such these cases, the delocalised nature of the interaction is particularly evident, since it emerges as an intrinsic feature of the interaction. Conversely, comparing RDG isosurfaces characterised by a given, suitable RDG isovalue allows for a qualitative ranking of the interaction strength. Stronger interactions are characterised by small, disc-shaped RDG domains, whereas weaker and weaker interactions are progressively denoted by broader, multiform RDG domains, which possibly include more than one critical point (at least in the cases considered here).

In other works, the RDG descriptor has been applied, with reasonable success, also to IAM EDs,^[37,38] A key point is the extent and kind of information about NCI which is missing and that which is instead already stored and hidden in IAM thanks to the structural knowledge inherent to the model and the cumulative frozen-electron distribution of the system's composing atoms. This relevant issue has been recently addressed by us, and within the RDG approach, in a companion paper.^[51]

To conclude, we have provided here a powerful tool to investigate NCI from data derived only from experiment. Moreover, we have analysed in detail the chemical insights that such a tool can provide in dissecting some of the most typical competing intra- and intermolecular interactions leading to the observed molecular packing. It is foreseeable that the RDG-based NCI descriptor might be successfully applied to the study of weak interactions in proteins by using the increasingly available experimental structural and electron-density information coming from last-generation synchrotrons or, eventually, X-ray free-electron laser facilities.

Experimental Section

Multipole refinements: All experimental EDs were reconstructed by multipole refinements with the XD2006 program package.^[49] For the three cases considered, we started from previously published accurate single-crystal X-ray diffraction data,^[40-42] all obtained at $T \leq 100$ K (austdiol: 70 K, benzene and famotidine: 100 K). In the final least-squares models, we refined thermal parameters of non-hydrogen atoms and multipole coefficients up to $l=2$ for hydrogen and up to $l=4$ for the other atoms. For austdiol and famotidine, heavy-atom positions were also refined. In famotidine, the X-H distances (X=C, O, N) were kept fixed at the neutron diffraction estimates,^[74] whereas the thermal motion of the hydrogen atoms was modelled as anisotropic with the software SHADE2^[75] and kept fixed during the refinement. For austdiol, positions and thermal motion parameters of hydrogen atoms were constrained at the published values (see also Supporting Information S1). For benzene all atomic positions were maintained at the reported neutron estimates.^[40] All of the least-squares details, including final parameter values, as well as the R indices and complete statistics, are reported in Supporting Information S1.

Quantum mechanical calculations: The CRYSTAL06 code^[76] was employed throughout to obtain periodic wave functions. We selected the widely used DFT-B3LYP^[77] Hamiltonian with 6-311G** basis set.^[78] The geometries were constrained at the experimental ones. Full details of the bulk quantum mechanical calculations are reported in Supporting Information S2. An updated version of the program TOPOND98,^[79,80] inter-

faced to CRYSTAL06, was employed to perform the topological analysis of the periodic ED.

Acknowledgements

We thank the Danish National Research Foundation for partial funding of this work through the Center for Materials Crystallography (CMC). J.C.G. thanks the Spanish Ministry of Education for a postdoctoral grant.

- [1] J. Černý, P. Hobza, *Phys. Chem. Chem. Phys.* **2007**, *9*, 5291–5303.
- [2] A. L. Lehninger, D. L. Nelson, M. M. Cox, *Principles of Biochemistry*, 2nd ed., Worth Publishers, New York, **1993**.
- [3] N. Krishnamoorthy, M. A. H. A. Yacoub, S. N. Yaliraki, *Biomaterials* **2011**, *32*, 7275–7285.
- [4] A. Dutta, A. D. Jana, S. G. Gangopadhyay, K. Kumar Das, J. Marek, R. Marek, J. Brus, M. Ali, *Phys. Chem. Chem. Phys.* **2011**, *13*, 15845–15853.
- [5] A. Gavezzotti, *Molecular Aggregation. Structure Analysis and Molecular Simulation of Crystals and Liquids*, IUCr Monographs on Crystallography No. 19, Oxford University Press, Oxford, **2007**.
- [6] H. Fenniri, M. Packiarajan, K. L. Vidale, D. M. Sherman, K. Hallenga, K. V. Wood, J. G. Stonwell, *J. Am. Chem. Soc.* **2001**, *123*, 3854–3855.
- [7] S. Keinan, M. A. Ratner, T. J. Marks, *Chem. Phys. Lett.* **2004**, *392*, 291–296.
- [8] G. R. Desiraju, *Crystal Engineering, The Design of Organic Solids*, Elsevier, Amsterdam, **1989**.
- [9] G. M. Day, T. G. Cooper, A. J. Cruz-Cabeza, K. E. Hejczyk, H. L. Ammon, S. X. M. Boerriger, J. S. Tan, R. G. Della Valle, E. Venuti, J. Jose, S. R. Gadre, G. R. Desiraju, T. S. Thakur, B. P. van Eijck, J. C. Facelli, V. E. Bazterra, M. B. Ferraro, D. W. M. Hoffmann, M. A. Neumann, F. J. J. Leusen, J. Kendrick, S. L. Price, A. J. Misquitta, P. G. Karamertzanis, G. W. A. Welch, H. A. Scheraga, Y. A. Arnautova, M. U. Schmidt, J. van de Streek, A. K. Wolf, B. Schweizer, *Acta Crystallogr. Sect. B* **2009**, *65*, 527–543.
- [10] R. E. Rosenfield Jr, R. Parthasarathy, J. D. Dunitz, *J. Am. Chem. Soc.* **1977**, *99*, 4860–4862.
- [11] a) J. J. McKinnon, A. S. Mitchell, M. A. Spackman, *Chem. Eur. J.* **1998**, *4*, 2136–2141; b) L. Lo Presti, R. Soave, M. Longhi, E. Ortoleva, *Acta Crystallogr. Sect. B* **2009**, *66*, 527–543.
- [12] A. R. Oganov, *Modern Methods of Crystal Structure Predictions*, Wiley-VCH, Weinheim, **2011**.
- [13] I. G. Kaplan, *Intermolecular Interactions: Physical Picture, Computational Methods and Model Potentials*, Wiley, New York, **2006**.
- [14] C. Gatti, R. Bianchi, R. Destro, F. Merati, *J. Mol. Struct.: THEOCHEM* **1992**, *255*, 409–433.
- [15] A. Volkov, Y. Abramov, P. Coppens, C. Gatti, *Acta Crystallogr. Sect. A* **2000**, *56*, 332–339.
- [16] B. Engels, T. C. Schmidt, C. Gatti, T. Schirmeister, R. F. Fink, *Structure & Bonding* **2012**, *147*, 47–98.
- [17] E. Espinosa, E. Molins, C. Lecomte, *Chem. Phys. Lett.* **1998**, *285*, 170–173.
- [18] E. Espinosa, M. Souhassou, K. Lachekar, C. Lecomte, *Acta Crystallogr. Sect. B* **1999**, *55*, 563–572.
- [19] C. Gatti, E. May, R. Destro, F. Cargnoni, *J. Phys. Chem. A* **2002**, *106*, 2707–2720.
- [20] Q. Zhao, D. Feng, Y. Sun, J. Hao, Z. Cai, *Int. J. Quantum Chem.* **2011**, *111*, 3881–3887.
- [21] M. Palusiak, T. M. Krygowski, *Chem. Phys. Lett.* **2009**, *481*, 34–38.
- [22] Y. V. Nelyubina, K. A. Lyssenko, R. G. Kostyanovsky, D. A. Bakulin, M. Yu. Antipin, *Mendeleev Commun.* **2008**, *18*, 29–31.
- [23] Y. V. Nelyubina, I. V. Glukhov, M. Yu. Antipin, K. A. Lyssenko, *Chem. Commun.* **2010**, *46*, 3469–3471.
- [24] L. Lo Presti, A. Ellern, R. Destro, B. Lunelli, *J. Phys. Chem. A* **2009**, *113*, 3186–3196.
- [25] R. F. W. Bader, *Atoms In Molecules: A Quantum Theory*, Clarendon Press, Oxford, **1990**.
- [26] T. S. Koritsanszky, P. Coppens, *Chem. Rev.* **2001**, *101*, 1583–1627.
- [27] C. Gatti, *Z. Kristallogr.* **2005**, *220*, 399–457.
- [28] A bond path is by definition associated with the only two nuclei it connects, whereas bonding may involve more than two atoms, for instance, in three-centre, two-electron bonds or in most CH $\cdots\pi$ interactions, and not all pairs of involved atoms appear to be connected by a bond path.^[31] The bond path, in QTAIM, is the line of maximum density, with respect to any lateral displacement, linking two nuclei in an energy equilibrium configuration. The existence of a bond path yields a sufficient and necessary condition for the two atoms being linked by the bond path to be bonded to one another. The collection of bond paths defines the molecular graph, and hence the molecular structure.
- [29] L. J. Farrugia, C. Evans, M. Tegel, *J. Phys. Chem. A* **2006**, *110*, 7952–7961.
- [30] A. M. Pendás, E. Francisco, M. A. Blanco, C. Gatti, *Chem. Eur. J.* **2007**, *13*, 9362–9371.
- [31] R. Ponc, C. Gatti, *Inorg. Chem.* **2009**, *48*, 11024–11031.
- [32] By “delocalised” character we mean here that these interactions may involve, and to a different extent, more than two atoms, as can be revealed by using the so-called delocalisation indices^[36] or the Source Function descriptor.^[34,35] Clearly, also the bond path criterion takes into account the effect of the remaining atoms in the molecule/system, but only indirectly, through their contribution to defining the electron density and gradient at each point of the path.^[35]
- [33] For instance, Pendas et al.^[30] showed that when two pairs of atoms are competing for a bond path, the pair found to be linked is always the one with prevailing contribution of the (atomic pair) exchange energy density.
- [34] R. F. W. Bader, C. Gatti, *Chem. Phys. Lett.* **1998**, *287*, 233–238.
- [35] C. Gatti, *Structure & Bonding* **2012**, *147*, 193–285.
- [36] X. Fradera, M. A. Austen, R. F. W. Bader, *J. Phys. Chem. A* **1999**, *103*, 304–314.
- [37] E. R. Johnson, S. Keinan, P. Mori-Sanchez, J. Contreras-Garcia, A. J. Cohen, W. Yang, *J. Am. Chem. Soc.* **2010**, *132*, 6498–6506.
- [38] J. Contreras-García, W. J. Yang, E. R. Johnson, *J. Phys. Chem. A* **2011**, *115*, 12983–12990.
- [39] At variance with refs. [37] and [38], we prefer to use the term “NCI” only for non-covalent interactions, and not also to denote the method introduced in these works.
- [40] H.-S. Bürgi, S. C. Capelli, A. E. Goeta, J. A. K. Howard, M. A. Spackman, D. S. Yufit, *Chem. Eur. J.* **2002**, *8*, 3512–3521.
- [41] L. Lo Presti, R. Soave, R. Destro, *J. Phys. Chem. B* **2006**, *110*, 6405–6514.
- [42] J. Overgaard, D. E. Hibbs, *Acta Crystallogr. Sect. A* **2004**, *60*, 480–487.
- [43] A. Zupan, J. P. Perdew, K. Burke, M. Causà, *Int. J. Quantum Chem.* **1997**, *61*, 835–845.
- [44] A. Zupan, K. Burke, M. Ernzerhof, J. P. Perdew, *J. Chem. Phys.* **1997**, *106*, 10184–10193.
- [45] A. D. Becke in *Modern Electronic Structure Theory* (Ed.: D. R. Yarkony), World Scientific, River Edge, **1995**, pp. 1022–1046.
- [46] The RDG-based NCI index by Johnson et al. is currently used for investigating non-covalent interactions, but in principle, it can be equally well applied to the study of covalent bonds.
- [47] G. Saleh, C. Gatti, L. Lo Presti, unpublished results.
- [48] N. K. Hansen, P. Coppens, *Acta Crystallogr. Sect. A* **1978**, *34*, 909–921.
- [49] A. Volkov, P. Macchi, L. J. Farrugia, C. Gatti, P. Mallinson, T. Richter, T. Koritsanszky, XD2006-A Computer Program Package for Multipole Refinement, Topological Analysis of Charge Densities and Evaluation of Intermolecular Energies from Experimental and Theoretical Structure Factors, **2006**. See also <http://xd.chem.buffalo.edu/>.
- [50] For the adopted Hamiltonian and basis set, we found that low ED regions are generally estimated as having larger ED values by ab initio than by the multipole ED. See, for instance, the ED values at the BCPs reported in the Supporting Information Tables S5.1–S5.3.

- Obviously, this difference leads to higher RDG values when the multipole ED is used [Eq. (1)].
- [51] G. Saleh, C. Gatti, L. LoPresti, *Comput. Theor. Chem.* **2012**, in press, DOI: <http://dx.doi.org/10.1016/j.comptc.2012.07.014>.
- [52] L. Lo Presti, R. Soave, R. Destro, *Acta Crystallogr. Sect. C* **2003**, *59*, o199–o201.
- [53] C. Pratt Brock, *Acta Crystallogr. Sect. B* **2002**, *58*, 1025–1031.
- [54] U. Koch, P. L. A. Popelier, *J. Phys. Chem.* **1995**, *99*, 9747–9754.
- [55] J. F. Dobson, K. McLennan, A. Rubio, J. Wang, T. Gould, H. M. Lee, B. P. Dinte, *Aust. J. Chem.* **2001**, *54*, 513–527.
- [56] B. Civalleri, C. M. Zicovich-Wilson, L. Valenzano, P. Ugliengo, *CrystEngComm* **2008**, *10*, 405–410.
- [57] D. S. Sholl, J. A. Steckel, *Density Functional Theory: A Practical Introduction*, Wiley, New York, **2009**, p. 29.
- [58] See ref. [5], Chapter 12, and references therein.
- [59] M. J. Allen, D. Tozer, *J. Chem. Phys.* **2002**, *117*, 11113–11120.
- [60] Actually, the former is the only true quantum mechanical observable, whereas individual attractive and repulsive energy terms are not. In principle, any quantum mechanical or classical energy partitioning that retrieves the overall cohesive energy is valid. Therefore, there is no universal agreement on what recipe should be employed to highlight specific dispersive and steric contributions to the total energy.
- [61] R. F. W. Bader, *J. Phys. Chem. A* **2009**, *113*, 10391–10396.
- [62] R. F. W. Bader, *J. Phys. Chem. A* **2010**, *114*, 7431–7444.
- [63] G. R. Desiraju, A. Gavezzotti, *Acta Crystallogr. Sect. B* **1989**, *45*, 473–482.
- [64] M. Nishio, *Phys. Chem. Chem. Phys.* **2011**, *13*, 13873–13900.
- [65] Though not recovered, a set of six more or less bent, inequivalent H→C bond paths, would have clearly been a topologically possible alternative outcome.
- [66] Monopole net charges on the unique H atoms are all positive and equal among each other within one standard deviation. Bader's net charges for the unique H atoms are all positive and range from 0.085 (H2) to 0.122 (H1) up to 0.145 (H3) electrons.
- [67] For example, considering the intermolecular BCPs in the isolated pair geometry as the reference points, the ED increases from 0.00061 to 0.00280 e Å⁻³ on passing from the isolated pair to the crystal, whereas the ED gradient goes from 0 to 0.0062 e Å⁻⁴. In the latter case, the RDG becomes as large as 2.54, well above the 0.6 isovalue (see above) adopted in this work.
- [68] B. Hegedüs, P. Bod, K. Harsanyi, I. Peter, A. Kalman, L. Parkanyi, *J. Pharm. Biomed. Anal.* **1989**, *7*, 563–569.
- [69] G. Gilli, P. Gilli, *J. Mol. Struct.* **2000**, *552*, 1–12.
- [70] a) A. Savin, B. Silvi, F. Colonna, *Can. J. Chem.* **1996**, *74*, 1088–1096; b) M. Calatayud, J. Andrés, A. Beltrán, B. Silvi, *Theor. Chem. Acc.* **2001**, *105*, 299–308.
- [71] F. H. Allen, O. Kennard, D. G. Watson, L. Brammer, A. G. Orpen, R. Taylor, *J. Chem. Soc. Perkin Trans. 2* **1987**, S1–S19.
- [72] R. Destro, R. Soave, M. Barzaghi, L. Lo Presti, *Chem. Eur. J.* **2005**, *11*, 4621–4634.
- [73] T. A. Keith, R. F. W. Bader, Y. Aray, *Int. J. Quantum Chem.* **1996**, *57*, 183–198.
- [74] F. H. Allen, I. J. Bruno, *Acta Crystallogr. Sect. B* **2010**, *66*, 380–386.
- [75] A. Østergaard Madsen, *J. Appl. Crystallogr.* **2006**, *39*, 757–758
- [76] R. Dovesi, V. R. Saunders, C. Roetti, R. Orlando, C. M. Zicovich-Wilson, F. Pascale, B. Civalleri, K. Doll, N. M. Harrison, I. J. Bush, P. D'Arco, M. Llunell, *CRYSTAL06 User's Manual*, University of Torino, Torino, Italy, **2006**.
- [77] A. D. Becke, *J. Chem. Phys.* **1993**, *98*, 5648–5652.
- [78] R. Krishnan, J. S. Binkley, R. Seeger, J. A. Pople, *J. Chem. Phys.* **1980**, *72*, 650–654.
- [79] C. Gatti, TOPOND98, An Electron Density Topological Program For System Periodic In N (N=0–3)dimensions, User's Manual, CNR-ISTM, Milano, Italy, **1999**.
- [80] C. Gatti, V. R. Saunders, C. Roetti, *J. Chem. Phys.* **1994**, *101*, 10686–10696.
- [81] C. B. Hübschle, P. Luger, *J. Appl. Crystallogr.* **2006**, *39*, 901–904.

Received: April 16, 2012

Revised: July 24, 2012

Published online: October 4, 2012